Physical Scale Model Testing of a Flexible Membrane Wave Energy Converter: Videogrammetric…

Article *in* International Journal of Marine Energy · September 2017

DOI: 10.1016/j.ijome.2017.09.004

3 authors, including:

Jarrah Orphin
Australian Maritime College

Alan Fleming
University of Tasmania

ARTICLE IN PRESS

International Journal of Marine Energy xxx (2017) xxx–xxx

Contents lists available at ScienceDirect

International Journal of Marine Energy

journal homepage: www.elsevier.com/locate/ijome

Physical scale model testing of a flexible membrane wave energy converter: Videogrammetric analysis of membrane operation

Jarrah Orphin [a,*], Alan Fleming [a], Cam Algie [b]

[a] Australian Maritime College, University of Tasmania Launceston, Tasmania, Australia
[b] Bombora Wave Power Pty Ltd., Perth, Western Australia, Australia

ARTICLE INFO

Article history:
Received 1 May 2017
Revised 8 September 2017
Accepted 19 September 2017
Available online xxxx

Keywords:
Videogrammetry
Photogrammetry
Wave energy converters
Experiment
Flexible membrane

ABSTRACT

In small-scale testing of wave energy converters (WECs), a key focus is on characterising the interdependent relationship between the primary converter and simulated power take-off system. If primary conversion is via the deformation of a flexible material, this task often requires non-contact measurement. In this paper, we introduce the development of an underwater non-contact measurement technique called videogrammetry, and its novel application to characterise the primary converter operation of a flexible membrane WEC. The work was part of Bombora Wave Power's concept validation wave tank tests at 1:15 scale. Details of the WEC and how it works is followed by an in depth description on applying underwater videogrammetry. A qualitative and quantitative analysis of membrane operation in a regular wave case is provided and discussed in terms of absorbed energy and power production. Two data sets are compared in this analysis. One data set is from videogrammetry and the other is airflow measurement data (airflow induced in the system due to membrane deformation converts wave energy to mechanical energy). This comparison quantifies the accuracy of videogrammetry, and also serves to verify airflow measurements that were used to determine performance indicators of the WEC throughout the entire test campaign. The results compare reasonably well. Sources of uncertainty for videogrammetry are discussed and improvements suggested. Preliminary best practices for applying videogrammetry in wave energy experiments are provided.

1. Introduction

Renewable energy, aside from the environmental benefits, is increasingly making economic sense. Wave energy is a viable form of renewable energy. Its potential and many methods for extraction have been extensively studied [1–5]; however, the levelised cost of energy (LCOE) needs to reduce if wave energy is to become economical. A key driver for reducing LCOE is technology convergence. Unfortunately, the wave energy industry has not converged to one or even several technologies. Without a clear solution, new wave energy converter (WEC) concepts continue to emerge. The first major advance in validating a new concept involves undertaking small-scale tests in hydrodynamic facilities such as wave tanks [6]. A key

* Corresponding author.
E-mail address: Jarrah.Orphin@utas.edu.au (J. Orphin).

https://doi.org/10.1016/j.ijome.2017.09.004
2214-1669/

Please cite this article in press as: J. Orphin et al., Physical scale model testing of a flexible membrane wave energy converter: Videogrammetric analysis of membrane operation, International Journal of Marine Energy (2017), https://doi.org/10.1016/j.ijome.2017.09.004

requirement is to estimate the power produced by the WEC, which involves characterising the relationship between incident waves, the primary converter, and the simulated power take-off (PTO) system. Characterising the dynamic behaviour of the primary converter is crucial to understanding both its operation and the WEC operation overall. This paper is focused on the application of a novel measurement technique to characterise the primary converter of a flexible membrane WEC. The work was part of Australian company Bombora Wave Power's concept validation wave tank tests.

Before introducing the measurement technique and experimental investigation, we will first briefly describe the design and operation of the WEC concept (further details of the device and proof of concept works are provided in [7]). Fig. 1 shows Bombora Wave Power's WEC prototype at the time of experiments in 2015.

The Bombora WEC is a bottom-fixed, fully submerged pressure differential device. It uses a flexible membrane and air turbine generator (power take-off (PTO)) system to convert wave energy to electricity. The membrane has a series of twelve cells separated into diaphragms containing air (Fig. 2a and b). As a wave peak passes over the device, an increase in pressure deforms the membrane, causing cells to deflate sequentially, pumping enclosed air (Fig. 2c). This pressure differential drives compressed air into a supply duct and around the closed circuit, which is ducted through an air turbine-generator PTO. Once the air has done work on the turbine, airflow returns back to a cell (restoring force) to start the cycle again. The full-scale device therefore operates in uni-directional flow.

Like many WECs, understanding the dynamic behaviour of the primary converter is crucial to understanding how the WEC produces power, and enabling future optimisation. In small-scale experiments, it is often necessary to quantify and qualify the primary converter operation in separate ways for verification of power estimates. Moreover, there is a lot value in obtaining as much information as practicable about the WEC system and subsystems in small-scale tests, where costs and timelines are relatively small. In the case of Bombora's small-scale experiments, characterising the flexible membrane operation required developing an underwater videogrammetry technique. This non-contact measurement approach was necessary due to the delicate nature of the membrane, whose dynamics would be greatly influenced if motion sensors were attached (i.e. accelerometers).

Videogrammetry is based on the principles of photogrammetry. Photogrammetry is essentially a method of making measurements from photographs [8]. By taking photos of an object or scene from different perspectives, a 3D reconstruction is possible from 2D photographs. Photogrammetry was developed for terrestrial mapping and surveying [9], but it is increasingly becoming a useful tool across many engineering disciplines to acquire accurate measurements of structures [10]. The technique has been proven accurate and reliable through developments made in space research into gossamer (flexible) structures [11–13]. Subsequent other demonstrations have emerged, for example in sail-boat research [14], where the authors apply photogrammetric modeling to empirically derive static shapes of a flying spinnaker in a wind tunnel. Using a number of fixed video cameras with a common field of view, dynamic measurement of an object or scene is possible, hence the term 'videogrammetry'. A 4D model (xyz + time) is the output of videogrammetric modelling. The technique is capable of monitoring dynamic structures that have displacements in the order of their size [10].

In the wave energy context, researchers at the Australian Maritime College (AMC), a specialist institute of the University of Tasmania, are applying videogrammetry to derive temporal and spatial maps of free surface wave fields produced by WEC radiation and diffraction effects [15–17]. Furthermore, videogrammetry has strong potential to replace current methods of measuring wave elevations using point-located wave probes [18].

Several technical components govern the successful application of photogrammetry. The following points list these components and related technical parameters, which have been adapted from [10] for videogrammetric modeling for wave energy experiments (Table 1).

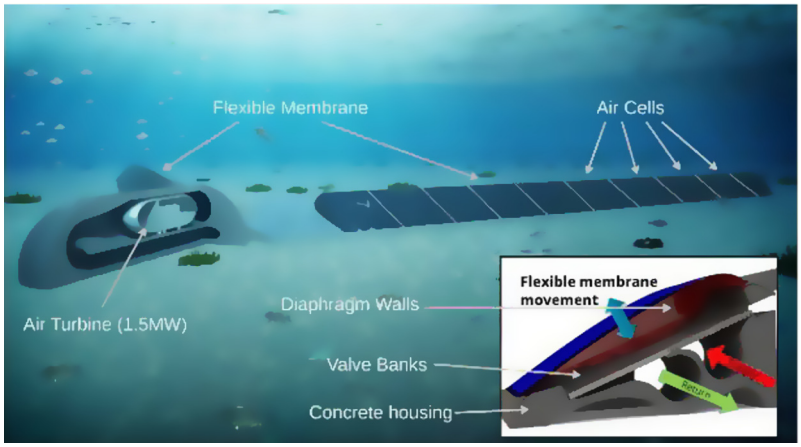

Fig. 1. Render of Bombora Wave Power's flexible membrane WEC prototype [7].

Please cite this article in press as: J. Orphin et al., Physical scale model testing of a flexible membrane wave energy converter: Videogrammetric analysis of membrane operation, International Journal of Marine Energy (2017), https://doi.org/10.1016/j.ijome.2017.09.004

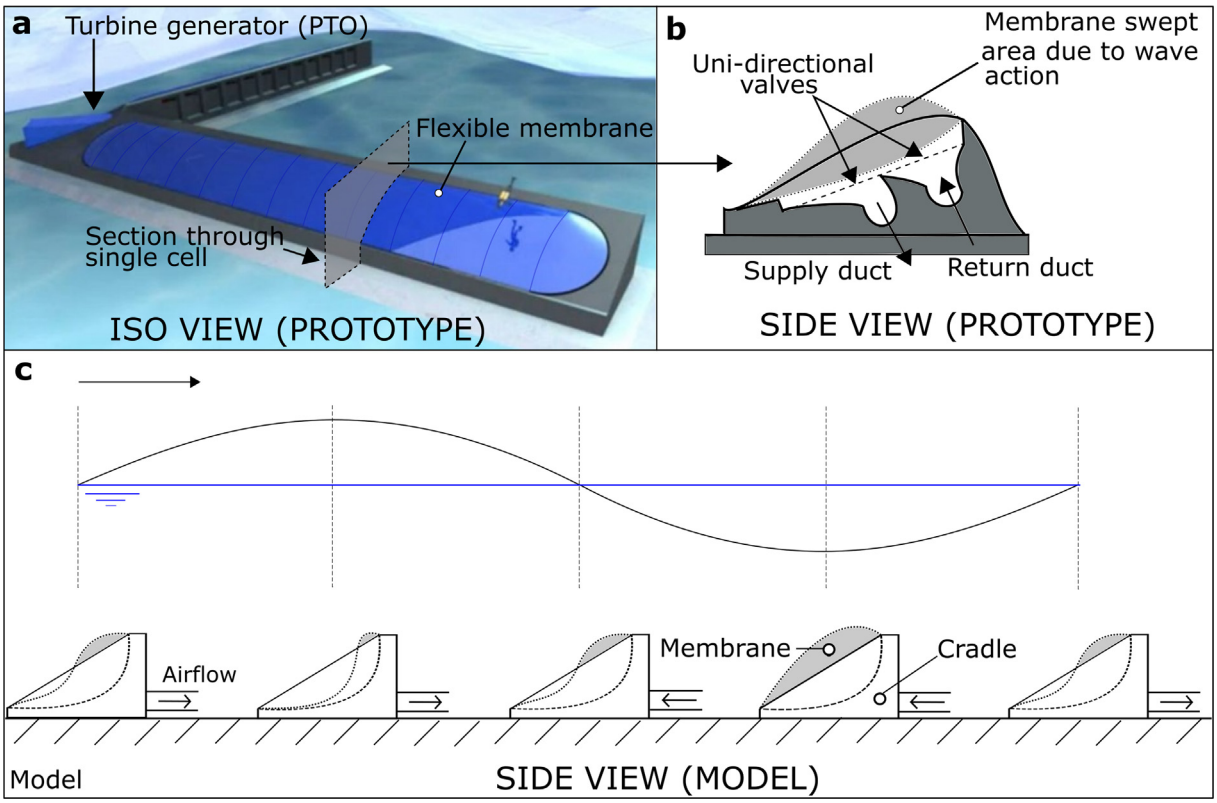

Fig. 2. (a) The Bombora prototype. (b) Device geometry with section view of single cell [7]. (c) Illustration of idealised cell deformation and resulting airflow over one wave period (representative of membrane operation).

Table 1
Technical components and related variables for videogrammetric modeling.

Component	Variables
Cameras	Resolution, camera stability, acquisition speed and data transfer, synchronisation, underwater hardware, real-time video recording
Targets	Suitable representation of static/dynamic object, coded and non-coded target placement and size, materials (paint, sticker), dot marking method (physical, projected)
Image configuration	Coordinate system, desired accuracy, number of cameras, location and orientation of cameras, calibration technique, object illumination
Image processing & 3D reconstruction	Image editing, manual and automatic marking, target identification and referencing (photogrammetry software), 3D model preparation for export to data analysis software
Model analysis	Handling outliers, surface fitting, desired data output, measurement accuracy and uncertainty

Evidently, videogrammetry is a technically demanding task. Research outcomes can be considerably affected by experimental setup, execution and post-processing. Nevertheless, careful consideration and implementation will enable accurate, quick and relatively cheap means to measure any structure or surface, moving or stationary [10].

This work has two primary aims. The first aim is the development of a novel underwater videogrammetry technique (Sections 2 and 3). The second aim is to characterise the membrane deformation of a flexible membrane WEC (Section 4). To achieve the second aim, we acquired qualitative (visual) and quantitative (measurement) videogrammetric data to characterise membrane operation in a simple wave condition. Additionally, videogrammetry enabled a separate method of estimating power produced by the WEC (Section 4.2 presents comparison of results). This serves to verify power estimate results from the primary method, which was via the measurement of airflow in each cell of the membrane. In so doing, a confidence interval for power estimates is created for other wave conditions and device variations in the campaign, for example different damping settings and system pressure. As this is the first application of videogrammetry in wave energy experiments, we provide preliminary best practices for using the technique, and recommendations for improving accuracy in future investigations (Section 5).

Please cite this article in press as: J. Orphin et al., Physical scale model testing of a flexible membrane wave energy converter: Videogrammetric analysis of membrane operation, International Journal of Marine Energy (2017), https://doi.org/10.1016/j.ijome.2017.09.004

2. Photogrammetry theory

Here we provide a brief overview of the theory behind photogrammetry. Photogrammetry theory is based on the relationship between image and object space, called exterior orientation. The aim is to determine the camera position in the object coordinate system. Position of the camera is determined by the location of its perspective centre (xyz) and by its attitude, expressed by three independent angles (ωφκ). A collinearity model can solve these six orientation parameters of the camera. The model relies on the condition that the perspective centre C, the object point P_o, and the image point P_i all lie on a straight line [19] (Fig. 3).

3D reconstruction of 2D images of object points is possible through solving the following collinearity condition equations:

$$x = -c\frac{(X_P - X_C)r_{11} + (Y_P - Y_C)r_{12} + (Z_P - Z_C)r_{13}}{(X_P - X_C)r_{31} + (Y_P - Y_C)r_{32} + (Z_P - Z_C)r_{33}} \tag{1}$$

$$y = -c\frac{(X_P - X_C)r_{21} + (Y_P - Y_C)r_{22} + (Z_P - Z_C)r_{23}}{(X_P - X_C)r_{31} + (Y_P - Y_C)r_{32} + (Z_P - Z_C)r_{33}} \tag{2}$$

with:

$$P_i = \begin{bmatrix} x \\ y \\ -f \end{bmatrix} \quad P = \begin{bmatrix} X_P \\ Y_P \\ Z_P \end{bmatrix} \quad c = \begin{bmatrix} X_C \\ Y_C \\ Z_C \end{bmatrix}$$

where x and y are the photo-coordinates in the image plane, c is the calibrated focal length, XP, YP, ZP are the object points, XC, YC, ZC and ω, φ, and κ are the unknown elements of exterior orientation (perspective centre and attitude angles, respectively), rij is the rotation matrix between the image and object planes. For a full derivation, see [19]. These simultaneous equations can be solved to compute the position of a point in 3D space by simple geometry if what is known is: (i) where the point is imaged on each photo, (ii) the parameters of the camera (focal length, lens distortion, etc.) from camera calibration, and (iii) the relative positions and angles of the camera when the photos were captured [20].

3. Methods

3.1. Experimental setup and tests

Physical experiments were conducted in the Australian Maritime College Model Test Basin. Fig. 4c shows a schematic of this facility including location of the test model (membrane only) and wave probes. Fig. 4b is a photo of the videogrammetry setup, depicting camera setup (angles, housing, and configuration). Fig. 4a illustrates the 1:15 scale model shown as partially submerged for the purpose of illustration, though all tests were undertaken when the membrane was full submerged, as seen in Fig. 2c. The pipes connect each cell to an 'added volume' to account for air compressibility. For this, large diameter PVC pipes were used as added volume chambers (see [7]). The device was installed at 45 degrees to the incident wave crest to

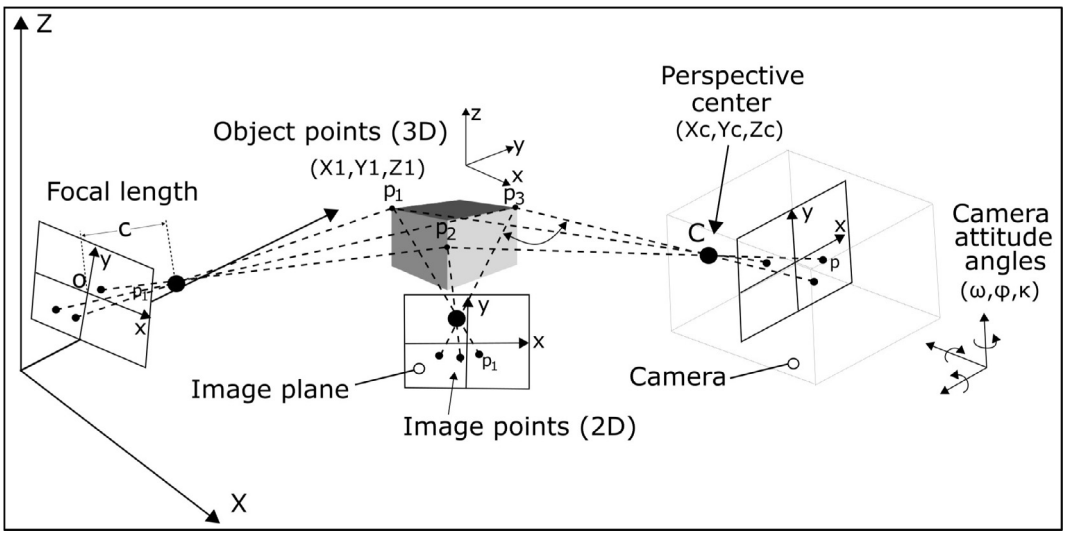

Fig. 3. Illustration of the collinearity condition for photogrammetry.

Please cite this article in press as: J. Orphin et al., Physical scale model testing of a flexible membrane wave energy converter: Videogrammetric analysis of membrane operation, International Journal of Marine Energy (2017), https://doi.org/10.1016/j.ijome.2017.09.004

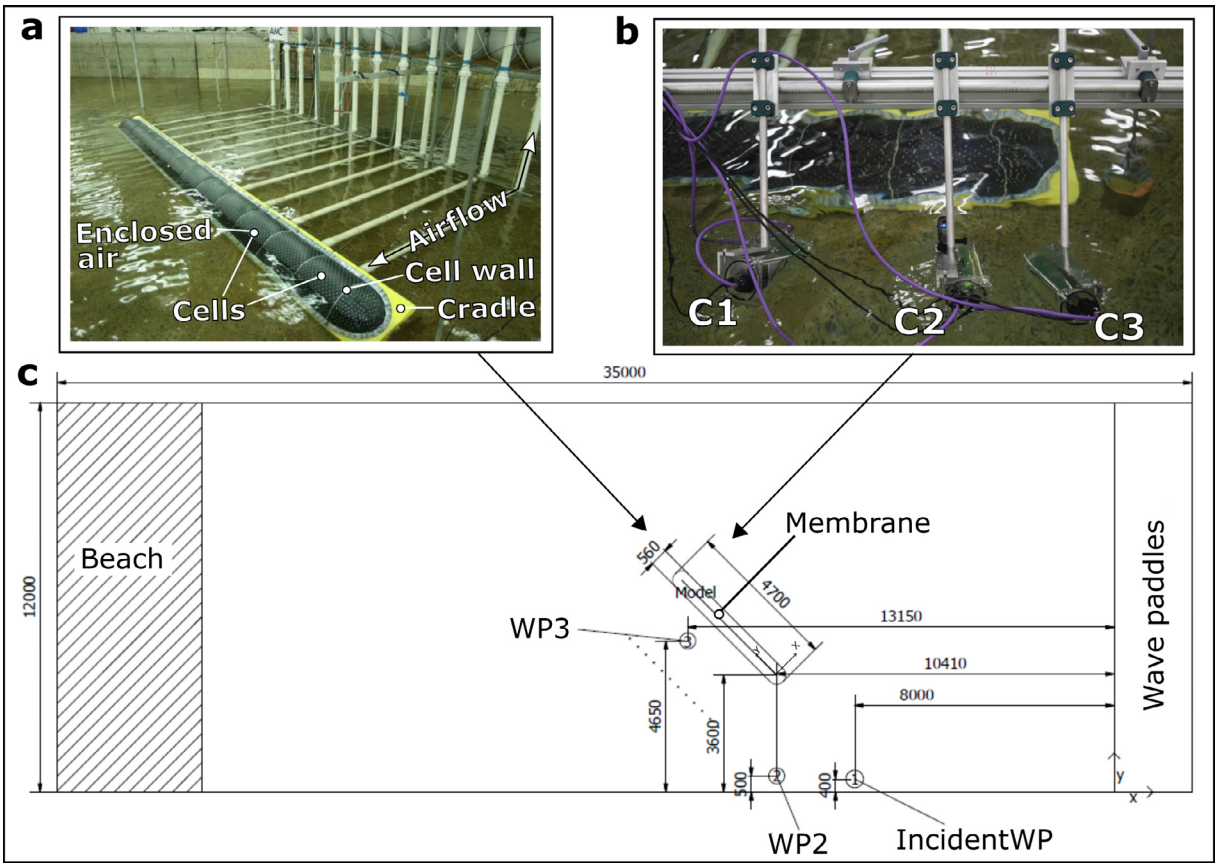

Fig. 4. (a) Setup of 1:15 scale model WEC with key features annotated. (NB: partially submerged membrane shown for illustration only, membrane was fully submerged during tests as depicted in Fig. 2c). (b) Setup of three-camera arrangement (C1, C2, C3) in underwater housings. (c) Plan view of locations of model (membrane only, at 45 degrees) and wave probes in the Australian Maritime College Model Test Basin.

Table 2
Test parameters and test case for the experiment.

Test parameter/case	Details
Regular waves	H = 0.167 m (2.5 m) T = 3.33 s (12.9 s)
Water depth	d = 0.72 m (10.8 m)
Test case	12 runs: one run for each of the twelve membrane cells (cameras recorded data one cell per run)

simulate the expected prototype configuration (Fig. 2a). It is noteworthy to remark that at model scale, airflow in the pipes is bi-directional. Membrane construction consisted of lightweight nylon ripstop material, fixed around its edges to the stationary fibreglass cradle structure, which had slits at the bottom to allow airflow through the pipe ducting (see Figs. 4a and 7). For each run, the pre-set volume in the system was such that on average each cell contained 50% of its total capacity of air.

Linearly calibrated S-type pitot tubes installed prior to orifice damper (orifice to pipe diameter ratio = 0.5) measured oscillating airflow velocity in the twelve ducts protruding from each individual cell. Likewise, pressure transducers were installed prior to and after the orifice to determine absorbed power.

Table 2 presents the test parameters and test case for the experiment. The regular wave condition was selected to minimise the downstream effects of the array of cameras on membrane dynamics (Fig. 4b). Noted, it is a typical wave height and period of the south-west Australian wave climate (The Bombora Wave Power company are located in Perth, Western Australia). See Appendix for complete details of the experiment (Table 6).

3.2. Videogrammetry method

The method of videogrammetry was adapted to acquire underwater measurements of membrane deformation. This measurement involved three stages. Fig. 5 shows a flow diagram that outlines the main components in the three-stage process. The sections following provide information on the method and materials associated with each component.

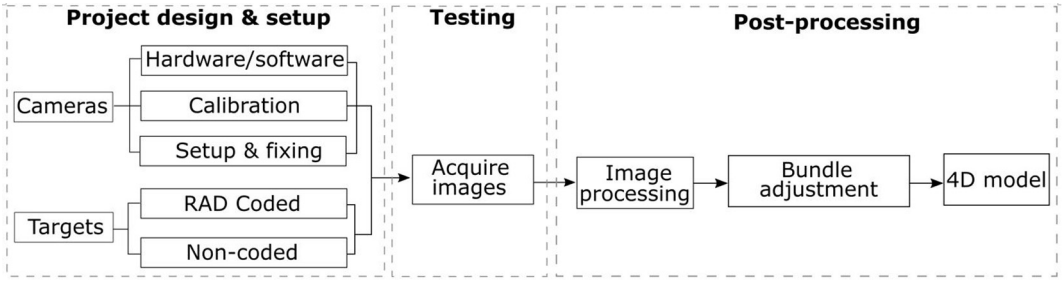

Fig. 5. Videogrammetry principle method, including key components of project design and setup, testing and post-processing. NB: 4D model is derived from 3D (xyz) measurement plus time (1D).

3.3. Cameras

Membrane motion was monitored by three digital video cameras of the same type (*iDS UI-3250CP-M-GL*), having a resolution of 1600 × 1200 pixels (2 megapixel) and a fixed focal length lens. Each camera was placed in waterproof housings. The cameras were connected to a PC using waterproof USB3 cables for image acquisition and multipurpose 6-pin cables for image synchronisation. A central hardware trigger synchronised image capture across the three cameras.

Each camera was calibrated underwater prior to tests, following the procedure documented by PhotoModeler [20]. Underwater calibration is necessary to maintain collinearity for underwater measurement (see Section 2). The output of calibration provides camera sensor format size (pixels), principal point (focal length) and lens distortion information for the photogrammetry software. It is noted that accurate calibration, and therefore accurate projects, depends on several factors, including (i) image coverage, ensuring that each photograph of the object is taken at a similar distance from the calibration grid, (ii) elevation angle of camera position, and (iii) camera focus, resolution and aperture settings.

Fig. 6 diagrammatically shows the experimental camera arrangement, which was designed to achieve good accuracy for dynamic measurements of membrane deformation. The yellow frustums depict the common field of view of each camera with convergent angles. There was an approximate 30° subtended angle between adjacent cameras. Camera orientations were chosen according to best practice specified by the photogrammetry software. Three cameras were employed to increase accuracy through photo redundancy (minimum of two cameras are needed for videogrammetry). One camera was fixed out of plane, ensuring a sufficiently large angle of elevation to capture the entire membrane deformation cycle. Camera zoom was set such that the entire membrane cell was maximised in the image. Camera depth of field settings were adjusted to ensure images of membrane deformation were in focus throughout the entire cycle. A horizontal aluminium frame was installed parallel to the front of the membrane for translation of the camera fixing system, such that image acquisition could be performed one cell at a time at a constant distance.

3.4. Targets

Targets are used in videogrammetric modelling for 3D point extraction. In this experiment, non-coded and coded targets were used. A black coloured membrane was prepared with high-contrast white non-coded targets, 4 mm in diameter, in a 20 mm × 20 mm rectilinear grid (Fig. 7). This produces a point-based representation of the membrane surface. Ringed automatically detected (RAD) coded targets [20] were placed around the stationary membrane edge. These individually unique RAD coded targets enable the photogrammetry software to automatically process the image sequences for 4D model reconstruction. Furthermore, RAD coded targets serve several purposes: the targets produce requirements for high-accuracy sub-pixel marking; they enable automatic referencing of targets between photos; they create a local co-ordinate frame; are efficient in solving spatial camera locations; and they enable the software to re-orient each image in the epoch for the scenario of any camera movement during image exposure. In this context, an epoch is defined as a group of images from multiple cameras corresponding to an instant in time.

3.5. Data processing

3.5.1. Videogrammetry

Minor processing of image sequences was completed prior to photogrammetric processing. Brightness, contrast and gamma correction were adjusted. The photogrammetry software used in this study, *PhotoModeler Motion* (PMM), is a graphical user interface based program that handles the 'bundle adjustment' processing (Section 2) [20]. Four main steps were required to process the image sequences of each cell to produce the 4D membrane model. First, image sequences were imported into the software. Second, an automatic marking algorithm marks every visible target across the three initial images to sub-pixel accuracy. A set of images taken at the same time are called an epoch. At least three different targets on each of the three images were manually matched, called 'referencing'. These three referenced points comprise the initial

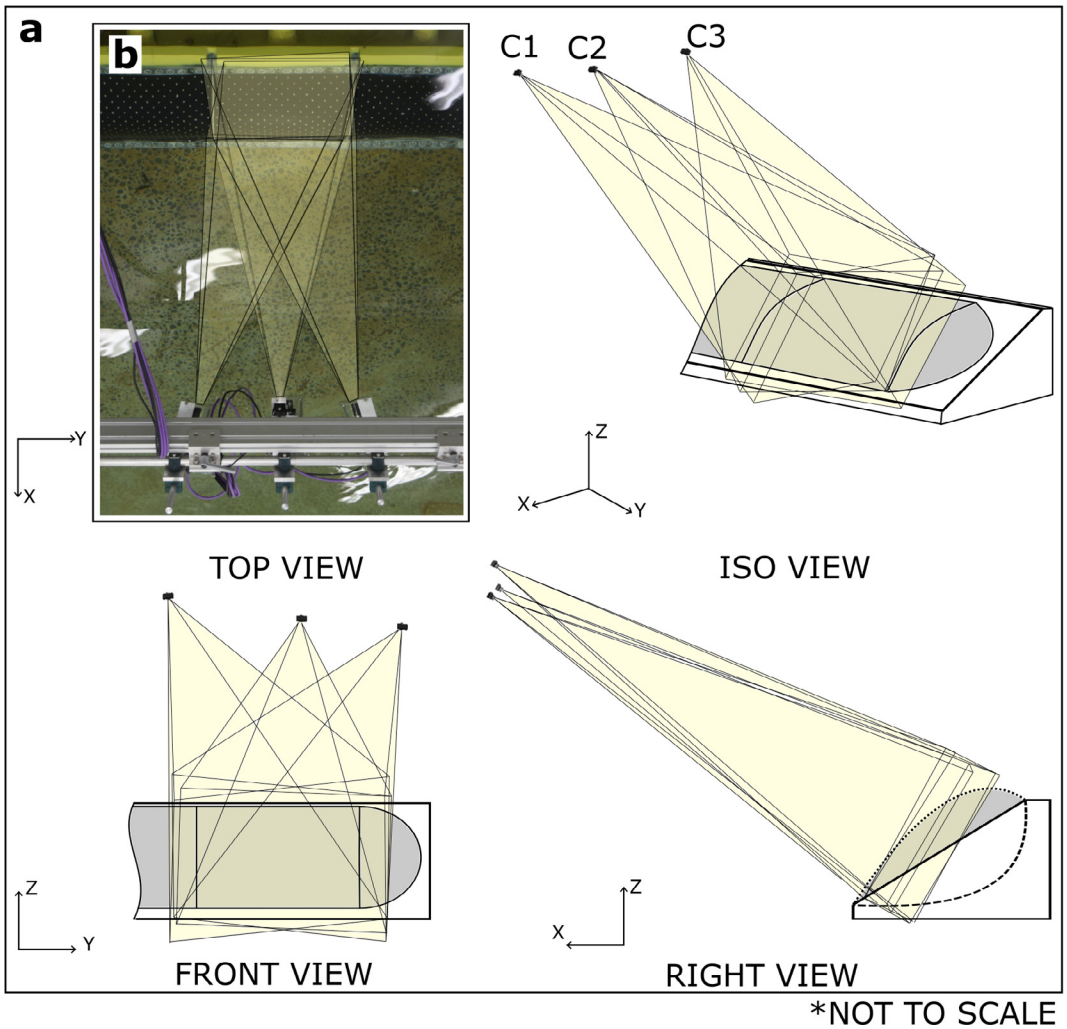

Fig. 6. (a) Schematic diagram of camera setup with frustums. (b) Inset showing a top view photograph of experimental camera setup. Relative camera positions (C1, C2, C3) remained constant for every run.

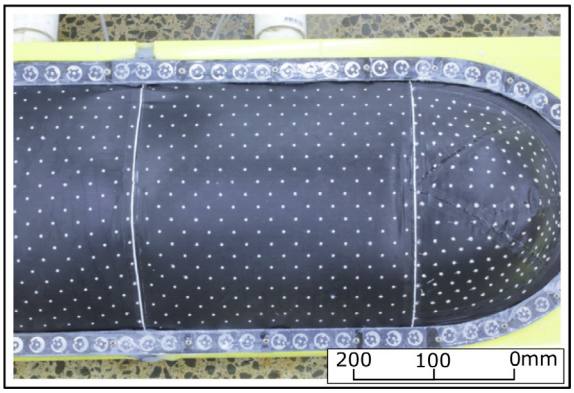

Fig. 7. Image of membrane marked with rectilinear grid of non-coded targets (dots, 4 mm diameter, 20 mm spacing) and stationary coded targets around the edges.

Please cite this article in press as: J. Orphin et al., Physical scale model testing of a flexible membrane wave energy converter: Videogrammetric analysis of membrane operation, International Journal of Marine Energy (2017), https://doi.org/10.1016/j.ijome.2017.09.004

3D points (xyz), which are relative to a defined coordinate system (XYZ). Third, the software uses these initial conditions to reference the remaining visible targets in the epoch and begin automatic 'bundle adjustment', which solves for the position of each referenced point and adjusts the 3D position solution until optimal. Each epoch in the video sequence is sequentially processed in the same manner, whereby points are tracked over time to produce 4D models of each cell. Finally, the time history 3D point data were exported to MATLAB for analysis.

A parameter that is useful for comparison of airflow and videogrammetry data is membrane cell volume change due to the interaction with waves. Cell volume was calculated differently for each method. From the airflow data, instantaneous cell volume V_A was determined by integrating the volumetric flow rate $Q_A = vA$, where v is airflow velocity measured by the S-Type pitot tubes and A the cross sectional area of the pipe ducts, such that:

$$V_A = \int_0^T Q_A(t)dt \tag{3}$$

From the videogrammetry data, cell volume was determined by calculating the difference between the surface of the membrane (interpolated from time series 3D point data) and the stationary cradle surface (Fig. 8). A double integral of each surface was used for the calculation, where the volume is enclosed by the assumption of a rigid vertical wall, which separates individual cells (y-axis limits in Fig. 8). In reality, the dividing vertical walls were flexible and thus experienced slight horizontal deformation during deflation/inflation, but the deflections averaged out over a complete wave period. The rigid wall assumption thus seems valid. Videogrammetry cell volume was calculated as follows:

$$V_{VG} = \int_{y_{\min}}^{y_{\max}} \int_{x_{\min}}^{x_{\max}} (f(x,y,z)_{cell} - f(x,y,z)_{cradle})dS \tag{4}$$

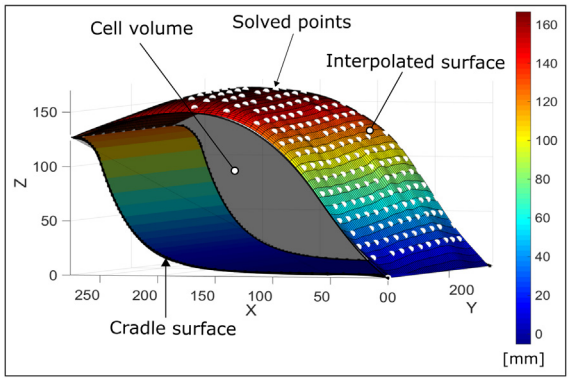

Fig. 8. Diagram of calculation for cell volume, with interpolated surface for solved points of one cell at one epoch. Grey region represents assumption of constant vertical wall (y-axis limits).

Subjecting each epoch to this double integral calculation produces videogrammetrically derived cell volume flux, suitable for direct comparison with the airflow derivation. Cell volume data were non-dimensionalised to percentage by dividing by the absolute maximum cell volume.Because cell volume changes over time, it is possible to determine volumetric flow rate Q_{VG} for videogrammetry data.

$$Q_{VG} = \frac{dV_{VG}}{dt} \tag{5}$$

Air pressure measured by a transducer in the pipe ducting before and after the orifice damper produces the requirements for calculating absorbed power P. Power is proportional to the product of volumetric flow rate Q and pressure P_c, such that $P = QP_c$. Therefore, power of the working fluid P_A (airflow) was determined in each cell across the orifice, and the absorbed power of the membrane cell P_{VG} as follows.

$$P_A = Q_A(P_1 - P_2) \tag{6}$$

and

$$P_{VG} = Q_{VG}(P_1 - P_2) \tag{7}$$

where P_1 and P_2 are the measured pressures in the pipe (pre-orifice) and added volume chamber (post-orifice), respectively.

These absorbed power values for each cell were non-dimensionalised with respect to the incident wave power per unit width P_I.

$$P_I = \frac{1}{2}\eta^2 \rho g C_g L \tag{8}$$

where η is wave amplitude, ρ is the water density, g is gravitational acceleration, Cg is the group velocity and L is the characteristic length of each cell, which is the width b of the cell relative to the wave crest, such that $L = b.\cos(45)$ due to the 45 degree orientation of the device.

A common non-dimensional parameter for quantifying the efficiency of a WEC and for making device-to-device comparisons is the capture width ratio. Assuming the incident wave amplitude is constant along the length of the membrane, the relationship between absorbed power of the membrane and the incident wave power is:

$$P_w = \frac{P_{A,VG}}{P_I} \tag{9}$$

As capture width incorporates a characteristic length, P_W can be determined at both an individual cell level and membrane level, as is shown in the power results (Section 4.2.3).

3.5.2. Measurement uncertainty

Repeatability uncertainty was evaluated in all results by calculating the standard deviation of amplitudes of individual waves ([21] shows repeatability can be quantified using individual regular waves). Three wave phases were considered to be in the stationary region, thus three samples (q_k) were taken. The standard deviation s of the n repeated readings was calculated using Eq. (10), taken from [22].

$$s = \sqrt{\frac{\sum_{k=1}^{n}(q_k - \bar{q})^2}{n-1}} \tag{10}$$

where q_k is the kth repeated reading and $\bar{q}$ is the mean value of the whole repeated reading. Assuming normal probability density function, a coverage factor of $k = 2$ was used corresponding to a 95% confidence level, thus error bars on the plots correspond to ± 1 standard deviation.

The accuracy of videogrammetry data were checked a number of ways. First, quantifying camera calibration determined the accuracy in terms of residual RMS and photo coverage. Residual RMS is the distance between where the point was marked (by user or automatically) on a photo and where the projection of the 3D point, associated with that marked point, falls on the photo [20]. Photo coverage refers to the coverage of the calibration grid within the set of calibration images (Table 4). Second, a true accuracy check was performed using an external data source (as specified by [20]). To this effect, on three separate days the distance between distinct points of each cell was measured with a tape measure. In PhotoModeler, measurements were taken of the same distinct points for three randomly selected epochs in the project. The mean of these measurements with corresponding standard deviations are listed in Section 4.3 (Table 5) in the form [mean value ± standard deviation]. The distance of the 'true' measurement (external) was compared with the PhotoModeler measurement to produce the measurement 'error'. Third, internal accuracy checks were undertaken, whereby residual error information contained the PhotoModeler project was analysed (Table 5). Residuals were then used to determine relative accuracy, which is in the form of "1 part in NNN".

3.5.3. Conventions

The following conventions apply to Section 4. The naming convention of cells follows that incident waves reach Cell 1 first (upwave) and Cell 12 last (downwave) due to the 45° orientation of the membrane to incident waves (Fig. 4c). Positive cell deformation is according to the coordinate system seen in Fig. 4; that is, positive cell deformation is along the positive x-axis, described as the cell inflating back to an un-deformed state. Negative deformation is therefore such that the cell is being deformed by the wave peak, i.e. compressed.

4. Results and discussion

The results and discussion includes three parts, and are discussed in the context of the wave tested. First, a qualitative analysis of global membrane behaviour for the wave tested is discussed using videogrammetry results. Second, a quantitative comparison of airflow and videogrammetry results with respect to cell volume, volume of flow and absorbed power of the membrane is provided. Measurement uncertainty results are presented in the third part.

4.1. Membrane characterisation: qualitative

Global membrane behaviour is a function of wave steepness, device settings (damping and system pressure) and configuration (water depth and orientation). Fig. 9 shows a visual representation of membrane behaviour due to the regular wave tested, and provides a basis for discussion on the effect of wave steepness on behaviour. For the wave tested, at T_1, Cell 1 is fully deflated (compressed). Airflow velocity in Cell 1 is zero at this time. As time increases and the wave travels over the membrane, downwave cells are sequentially deformed, causing air to travel through the pipe in the negative x direction. At the same time, upwave cells are restored to an inflated state, as air travels in the positive x direction. After 3.33 s (wave period), the cycle begins again. For this wave, mid cells do not deform as much as end cells. To be clear, this uneven distri-

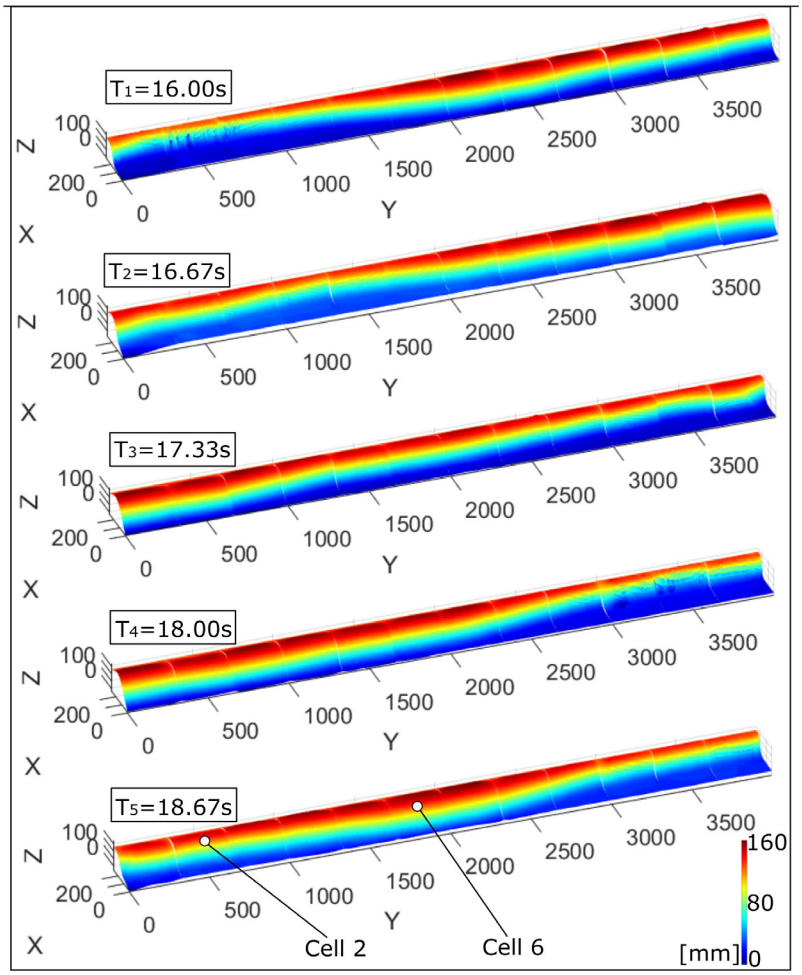

Fig. 9. Five plots representing global membrane behaviour due to one period of the regular wave tested. Coloured surface is an interpolated surface fit over videogrammetry point data.

bution of work across the cells is wave frequency dependent. Membrane dynamics (and thus device performance) depends on the ratio of wavelength to WEC length. For long period waves (wave length/WEC length ratio > 1) as is presented, end cells have a larger deformation cycle, due to the end cells having the greatest distance from the area centroid of the device. When this ratio is one, cell deformation is approximately equivalent across the membrane; that is, each cell contributes equally to the total device power. In light of these experimental results, the designers have since altered the prototype design to minimise wave frequency dependency by having two parallel banks of four cells (see [23] for details), instead of the 'V' configuration depicted in Fig. 1.

Fig. 10 compares local cell behaviour over one deformation cycle, showing the behaviour of two cells in different locations using videogrammetry data. Fig. 10a presents five surface plots of Cell 2 (A1-5) and Cell 6 (B1-5) that represent key points in the deformation cycle (cell locations are annotated in Fig. 9). A1-5 and B1-5 are annotated on the accompanying plot in Fig. 10b, which shows cell volume change over time. Maximum cell volume (100%) is equivalent between Cell 2 and Cell 6 (A2/B2) because each cell returns to the un-deformed state every wave period for the wave tested. Cell 2 minimum volume is 21% whereas Cell 6 is 50% (A4/B4). Therefore, change in cell volume during one wave period is 81% for Cell 2 and 50% for Cell 6. These observations highlight that a cell that deforms slightly more relative to another converts a noticeably larger amount of energy due to the change in volume characteristic.

4.2. Membrane characterisation: quantitative

4.2.1. Cell volume

Fig. 11 shows cell volume change for the selected time interval, including both the airflow (solid line) and videogrammetry (dashed line) data. Three out of a possible twelve membrane cells are shown as they are representative of global membrane dynamics and facilitate clarity. We will first discuss deformation behaviour of the cells, and then compare the results

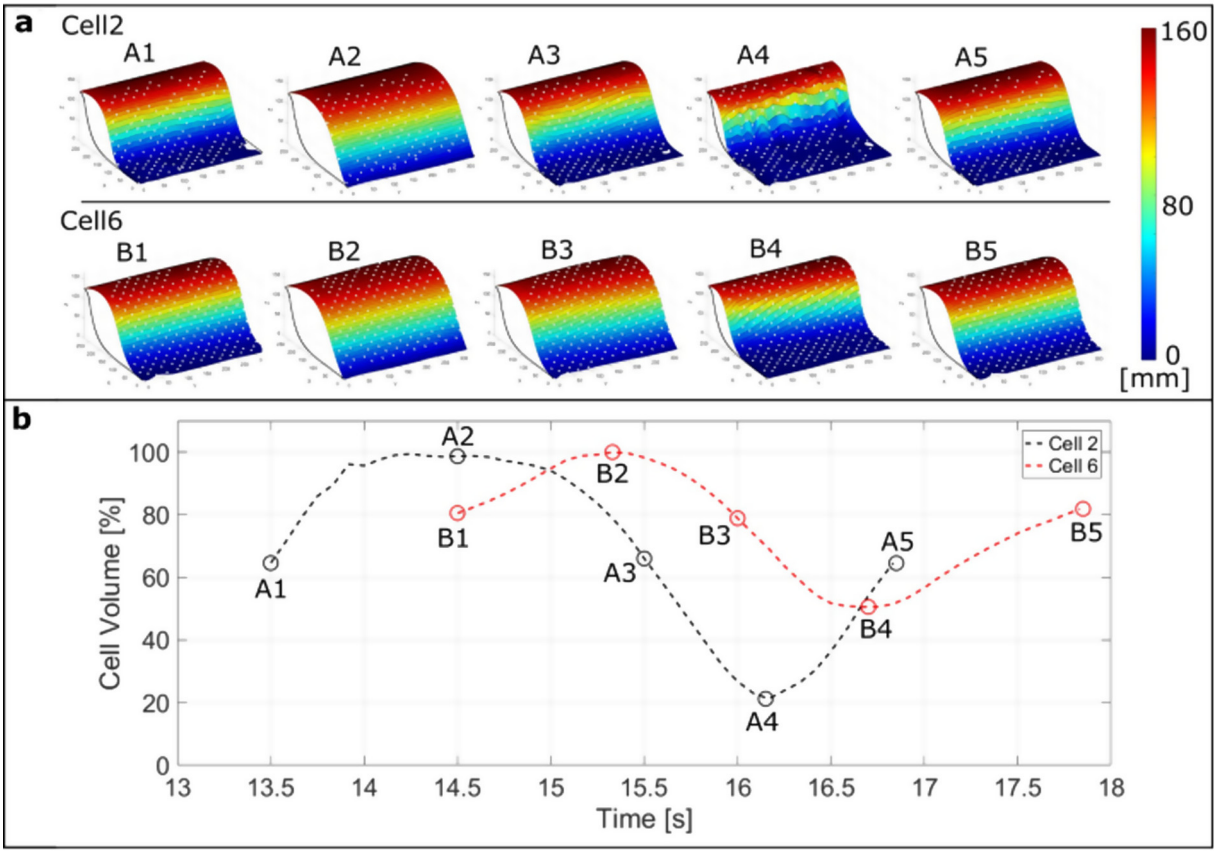

Fig. 10. (a) Surface plots of videogrammetry point data for Cell 2 and Cell 6 deformation cycle over one wave period. (b) Cell volume time series with distinct points annotated corresponding to Cell 2 and Cell 6 plots above.

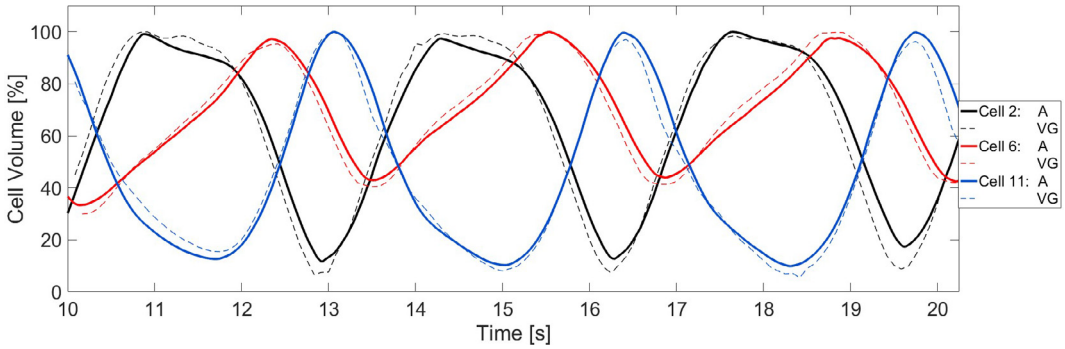

Fig. 11. Cell volume time series depicting three of twelve membrane cells (2, 6, and 11). Airflow (A) is shown as a solid line and videogrammetry (VG) a dashed line.

of both data sets. It can be observed that cell behaviour depends on its location in the membrane. Firstly, we see a phase shift between cell deformation. Relative to Cell 1, Cell 6 is approximately 90° and Cell 11 is 180° out of phase. This is due to the 45° membrane orientation (Fig.4c). In terms of power production, this natural phasing of the oscillatory wave excitation force is desirable for grid integration. Another interesting feature of these results is that while Cell 2 and Cell 11 have similar amplitudes, their deformation cycles are opposite. Cell 2 has a broad peak and narrow trough, whereas Cell 11 is the opposite. In other words, Cell 2 is inflated longer relative to Cell 1. In the full-scale device, the effect of different cell inflation and deflation behaviours is minimised due to air from each cell being pumped into a common supply duct, thus averaging the variations.

Comparison of the data sets indicate the cell volume profiles fit reasonably well. While the trends fit closely, there is some discrepancy in the amplitudes. Cell 2 shows the largest difference in amplitude. The slight delay seen in the airflow data is attributed to the requirement to accelerate air in the ducting, which was a total of about 5 m long. Furthermore, for peak airflow a noticeable pressure drop is possible due to the fluid inertia. This influences pressure-flow characteristics in the system, causing non-linear effects that would not be captured by the linear pitot tubes measuring airflow. The slight noise seen at the peak cell volume of Cell 2 in the videogrammetry data is due to membrane wobble, which is caused by air flying out of the pipe and filling the cell in a turbulent manner. Another way to compare the data sets is by analysing the volume of flow for a given wave period (in and out), as presented and discussed in the following section.

4.2.2. Volume of flow

Volume of flow is a measure of exchanged volume of air in each cell over one wave period. Fig. 12a compares phase-averaged volume of flow per wave cycle for airflow and videogrammetry data. Before discussing these results, it is first necessary to explain why Cell 1 and 12 show airflow data only. This is due to the design of the model and the videogrammetric measurement of membrane deformation cell by cell. For example, as seen in Fig. 7 the end of the membrane is a semi-circle end 'cap' that also contains air, which was approximately one quarter of air of the adjacent Cell 12. During the deformation cycle, air in the end cap travelled down the pipe duct of Cell 12. Airflow measured in this pipe was therefore a combination of both Cell 12 air and end cap air. The same is true for Cell 1. Videogrammetric measurement did not capture end cap deformations, therefore, videogrammetry data for Cell 1 and 12 are not shown for comparison of results, because it is not a true comparison.

For the wave tested the trend of exchanged volume decreases until Cell 7 and increases thereafter (Fig. 12a), which is reflected in Fig. 9. For comparison of volume of flow results, Fig. 12c shows the relative difference between data sets. For the upwave cells, there is an average positive relative difference of approximately 8%. Downwave cells show a similar value, though negative relative difference. Cell 8 shows the largest difference of −14%. The trend of positive relative difference for upwave cells and negative for downwave cells is likely due to dynamic pressure-flow interactions in the downwave cells caused by upwave cells.

4.2.3. Power

Capture width at an individual cell level is shown in Fig. 12b for both data sets. This analysis in terms of capture width is intended for comparative purposes, rather than to characterise the performance of the device, which would require a full

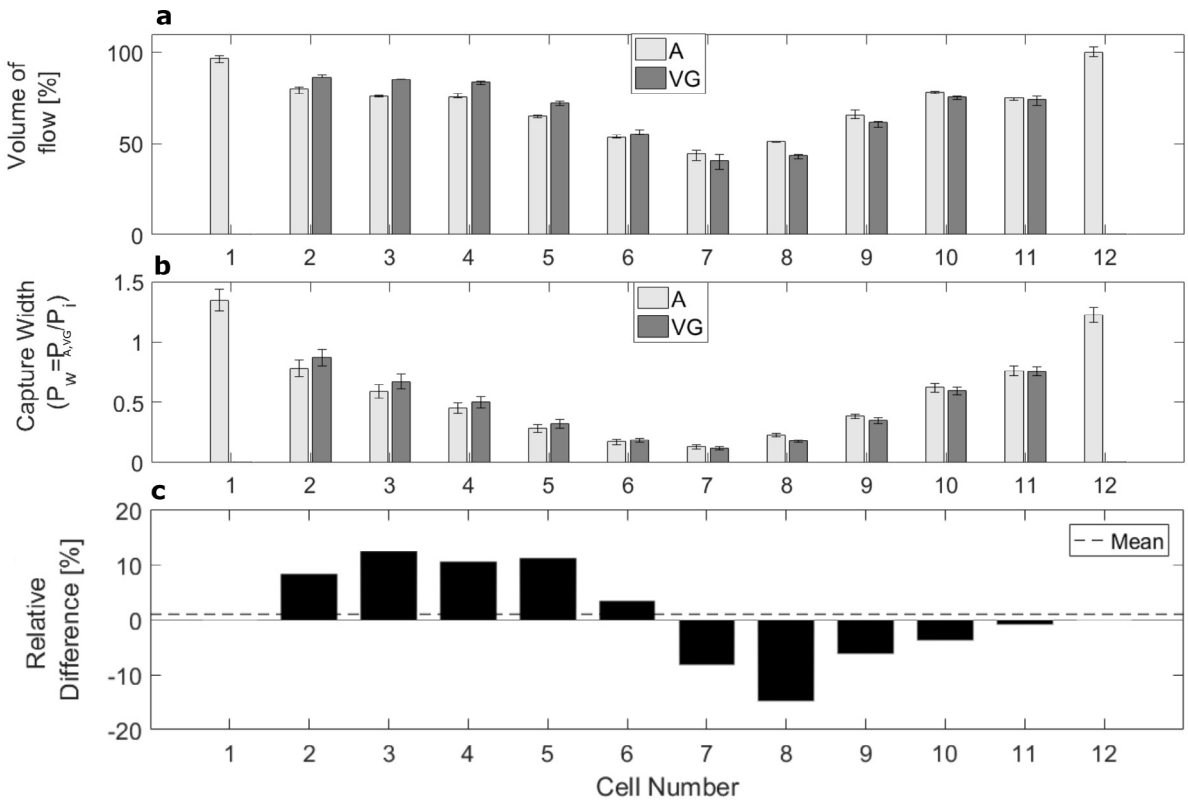

Fig. 12. (a) Average airflow (A) and videogrammetry (VG) volume of flow. Error bars represent one standard deviation with a confidence interval of 95%. (b) Average airflow and videogrammetry capture width. (c) Relative difference between results.

Please cite this article in press as: J. Orphin et al., Physical scale model testing of a flexible membrane wave energy converter: Videogrammetric analysis of membrane operation, International Journal of Marine Energy (2017), https://doi.org/10.1016/j.ijome.2017.09.004

power matrix. The general quadratic-like trend across the twelve cells is similar to the volume of flow results above, albeit more pronounced. This is due to instantaneous power being a function of volumetric flow rate and pressure, which are in phase and multiplied. This results in the observed trend. For the wave tested, Cell 1 capture width shows the largest value of 1.35, whereas Cell 7 produced the minimum mean value of 0.15. The mean capture width across all cells was 0.58 (airflow data). A capture width value larger than one is possible in this condition due to energy being absorbed during both negative and positive cell deformation (bi-directional flow).

The device produces power during both negative and positive cell deformation, manifest in a dual-peaked power profile over one wave period (Fig. 13). In both instances of deflection, power is positive because volumetric flow rate and pressure are in phase. At the cell level, Cell 2 exhibits the largest absorbed power of 63% for both data sets, seen at the first peak (Fig. 13a). It is noted that Cell 1, not shown, produced the greatest absorbed power, equivalent to the maximum incident wave power at 100%. Inspecting plot (a), the first peak corresponds to the maximum volumetric flow rate and pressure combination for the wave phase, occurring when the cell is half way through negative deformation (compression). The first trough marks a completely deformed state (minimum volume). The second peak corresponds to half way of positive deformation. The second longer trough where no power is absorbed corresponds to the time when the cell is un-deformed, with full volume. For Cell 2, these peaks are approximately equivalent, as is the case for Cell 11. In real terms, these end cells produce equal power during negative and positive cell deformation. Cell 4 and Cell 9, on the other hand, exhibit a larger value for negative cell deflection, with Cell 4 producing approximately twice the power relative to its positive deflection. This leaves Cell 6 virtually single peaked such that power is only extracted during negative deflection. The videogrammetry and airflow data show similar absorbed power profiles at both the cell level and membrane level.

For the wave tested, the device extracts approximately 40% more power when the membrane is being deformed compared to when the membrane is being restored back to the un-deformed state (Fig. 13b). Although the time series data sets show little discrepancy, videogrammetry data has pronounced peaks and troughs. Airflow data produced the largest measure of absorbed power, quantified in the capture width results shown in Table 3. 7.1% difference between data sets was observed. It is noted that Cell 1 and Cell 12 data were included in this capture width calculation for the device, which attributes to the smaller value observed for videogrammetry due to the reason detailed in Section 4.2.2.

The comparisons presented provide sufficient verification for the airflow data, insofar as the estimates of airflow in other wave conditions tested throughout the concept validation campaign should be within the vicinity of ±10%. We infer this value by taking into account both volume of flow and power results. For concept validation tests, this degree of uncertainty

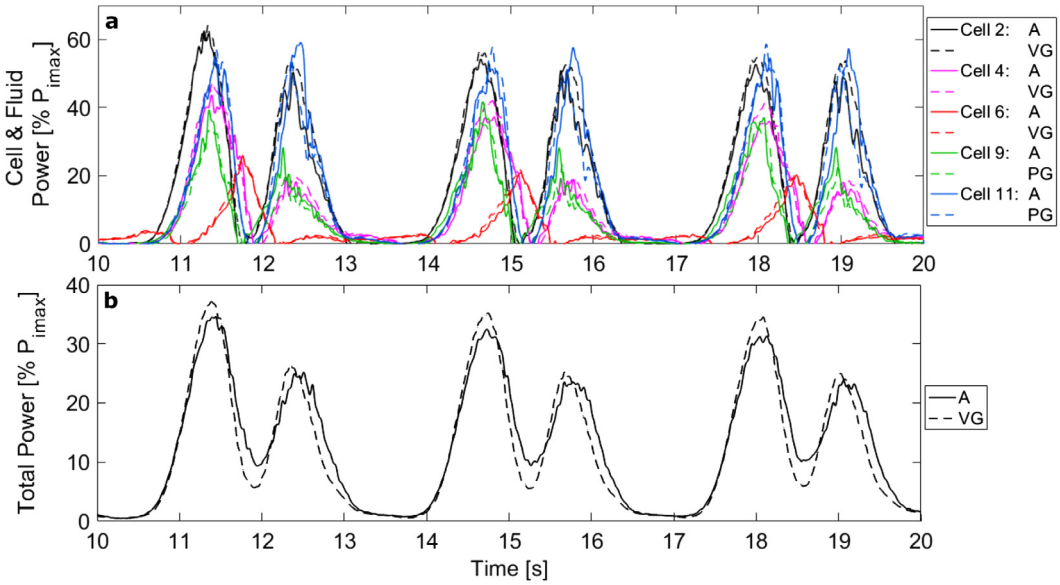

Fig. 13. (a) Time series of power of selected membrane cells (Cell, VG) and airflow (Fluid, A), non-dimensionalised w.r.t maximum incident wave power. (b) Membrane absorbed power (sum of the power of each cell) non-dimensionalised w.r.t maximum incident wave power sum.

Table 3
Capture width.

	Airflow	Videogrammetry	Difference [%]
Capture width	0.58	0.54	7.1%

Please cite this article in press as: J. Orphin et al., Physical scale model testing of a flexible membrane wave energy converter: Videogrammetric analysis of membrane operation, International Journal of Marine Energy (2017), https://doi.org/10.1016/j.ijome.2017.09.004

is acceptable. This assumes the videogrammetry data are of sufficient quality, which is shown to be the case in Section 4.3 (Table 5).

4.3. Experimental uncertainty

To quantify videogrammetry measurement uncertainty, we performed both internal and external accuracy checks. For internal accuracy, each of the three cameras were calibrated to a medium-high quality (Table 4). Residual RMS results are low, with a mean of 0.28 mm and maximum of 0.33 mm. High photo coverage was obtained, with a mean value of 90% and minimum of 88%. These calibration results indicate a strong 'project' [20].

The external accuracy checks (Table 5), determined using the method described in Section 3.5.2 are relatively low, with a maximum of 1.3% error. The internal accuracy results eventuate to a mean relative accuracy of one part in 2370 (1:2371), which is comparable to the investigations presented in [12,13,24] considering the experimental set up. This degree of uncertainty for videogrammetry measurement is acceptable given the scope of the experiment and the stage of WEC development.

Other possible sources of videogrammetry measurement uncertainty that may have influenced the accuracy of results include image distortion due to the underwater camera housing in which each camera was situated; slight camera movement due to pressure fluctuations of passing waves (not visually observed in the experiment); and large membrane deformation relatively to its size. Overall, we surmise these uncertainties did not have any significant influence on the results.

Other sources of experimental uncertainty may have influence test results. Considering the stage of WEC testing, it was unnecessary to quantify these. However, future experimental investigations ought to consider the following sources of uncertainty: geometry uncertainty (membrane material and cradle construction, pipes ducts), installation uncertainty (device orientation), calibration uncertainty (sensors), measurement uncertainty (method of measurement) and data reduction uncertainty (propagation of uncertainties, facility bias).

Table 4
Camera calibration results.

Camera	Residual RMS [mm]	Photo coverage [%]
1	0.18	88
2	0.33	91
3	0.33	91

Table 5
Videogrammetry measurement uncertainty.

Cell	External accuracy check			Internal accuracy check	
	Tape measured [mm]	PhotoModeler measured [mm]	Error [%]	Mean RMS residual [mm]	Relative accuracy [mm/mm]
1	329.8 ± 0.4	331.5 ± 0.9	0.5	0.15	1:2533
2	297.3 ± 0.4	296.3 ± 0.6	−0.3	0.14	1:2714
3	310.0 ± 0.1	311.3 ± 0.6	0.4	0.15	1:2533
4	310.1 ± 0.1	314.0 ± 0.0	1.3	0.16	1:2375
5	305.1 ± 0.1	305.3 ± 0.6	0.1	0.20	1:1900
6	314.4 ± 0.6	314.3 ± 0.6	0.0	0.13	1:2923
7	294.1 ± 0.1	293.3 ± 0.6	−0.3	0.26	1:1462
8	326.0 ± 0.1	325.7 ± 0.6	−0.1	0.15	1:2533
9	301.3 ± 0.4	301.0 ± 0.0	−0.1	0.16	1:2375
10	306.4 ± 0.6	306.3 ± 0.6	0.0	0.16	1:2375
11	295.8 ± 1.0	296.3 ± 1.2	0.2	0.13	1:2923
12	324.4 ± 0.6	324.0 ± 0.0	−0.1	0.21	1:1810

5. Conclusions

In this work, an underwater videogrammetry technique was applied to characterise the Bombora WEC membrane operation, and verify airflow data. A key focus of the paper was on providing extensive information on the method of videogrammetry and its application in making dynamic measurements of membrane deformation. A qualitative and quantitative analysis of membrane operation was presented and discussed in terms of airflow and device power. Furthermore, we introduced a robust non-contact measurement technique to the wave energy model test community, which has advantages in overcoming technical barriers in and improving the quality of wave energy experiments. The following conclusions are drawn from this study.

- Demonstrated a novel application of underwater videogrammetry. A videogrammetry measurement uncertainty analysis was undertaken through internal and external accuracy checks, where a medium-high accuracy in the measurement was found.

- A qualitative analysis of global membrane behaviour and examples of local cell behaviour was presented using visual depictions generated by videogrammetry data.
- Membrane cell deformation was quantified with respect to cell volume flux, volume of flow, power, and capture width. The results of videogrammetry and airflow data sets were compared. They matched reasonably well considering it was a first application of underwater videogrammetry, and the degree of uncertainty tolerated in concept validation tests. A mean capture with of 0.58 (airflow data) was observed for the regular wave tested.

Regarding Bombora's WEC development, the outcomes of this study contribute in two primary ways. One is the generation of valuable empirical data for understanding membrane operation and system dynamics, which is also useful for input into future physical and numerical modelling optimisation. The other is the verification of airflow data for proof of concept requirements.

Here we provide a set of preliminary best practices for performing a high accuracy photogrammetry/videogrammetry project pertinent to marine renewable energy research (for detailed factors affecting accuracy, see [20]). They are:

- Photo resolution: 11+ mega pixels.
- Camera Calibration: use prescribed calibration grids, achieve more than 90% coverage, and calibrate in the same medium to that of the experiment.
- Angles between photos: for more accurately solved points, arrange cameras with at least 30 degree and preferably between 60 and 90 degree subtended angles.
- Photo orientation quality: 35+ points, with 50–80% coverage to increase accuracy in solving camera orientations (known to contribute noticeably to project accuracy).
- Camera fixity: install fully rigid system to ensure photo orientation quality.
- Photo redundancy: generally, more cameras produce greater accuracy.
- Targets: *retro*-reflective, appropriately placed coded and non-coded targets such that there is the correct balance between object representation and target detection.

Acknowledgments

Bombora Wave Power for their regular communication, support and documentation. Dr Jean-Roch Nadar for mathematical advice. Technical staff Kirk Meyer and Liam Honeychurch for videogrammetry equipment, setup and advice. Marie-Louise Taylor for editing.

This research did not receive any specific grant from funding agencies in the public, commercial, or not-for-profit sectors.

Appendix A. Experiment Summary Details

Table 6
Experiment summary.

Parameter	Description	
Model scale		1:15
Membrane	Length	4.4 m
	Aspect ratio	≈12:1
	No. of cells	12
	Angle to crest	45°
Test tank dimensions	Length	35 m
	Width	12 m
	Depth	0.72 m
Cell working volume		50%
Wave conditions	Type	Monochromatic (regular)
	Height	0.167 m
	Period	3.33 s
Measured variables	Wave amplitude	
	Airflow velocity and pressure	
	Cell deformation (videogrammetry)	
Cameras		3× iDS UI-3250 CP-M-GL
	Hardware/software	Underwater housings DAQ Synchronisation trigger
	Calibration	Manual; PMM grid; underwater
	Configuration	Convergent view ≈30°
Targets	Coded	RAD coded targets
	Non-coded	White dots (paint); 20 × 20 mm rectilinear grid
Photogrammetry processing	Photo	Modeler Motion

Please cite this article in press as: J. Orphin et al., Physical scale model testing of a flexible membrane wave energy converter: Videogrammetric analysis of membrane operation, International Journal of Marine Energy (2017), https://doi.org/10.1016/j.ijome.2017.09.004

References

[1] A. Clément, P. McCullen, A. Falcão, A. Fiorentino, F. Gardner, K. Hammarlund, G. Lemonis, T. Lewis, K. Nielsen, S. Petroncini, et al, Wave energy in Europe: current status and perspectives, Renew. Sust. Energy Rev. 6 (5) (2002) 405–431.
[2] J. Falnes, A review of wave-energy extraction, Mar. Struct. 20 (4) (2007) 185–201.
[3] B. Drew, A. Plummer, M.N. Sahinkaya, A review of wave energy converter technology, Proc. Inst. Mech. Eng. A 223 (8) (2009) 887–902.
[4] A.F.d.O. Falcão, Wave energy utilization: a review of the technologies, Renew. Sust. Energy Rev. 14 (3) (2010) 899–918.
[5] I. López, J. Andreu, S. Ceballos, I.M. de Alegría, I. Kortabarria, et al, Review of wave energy technologies and the necessary power-equipment, Renew. Sustain. Energy Rev. 27 (2013) 413–434.
[6] ITTC, Wave Energy Converter Model Test Experiments, In: 7.5-02-07-03.7.2014, International Towing Tank Conference.
[7] S. Ryan, C. Algie, G.J. Macfarlane, A.N. Fleming, I. Penesis, A. King, et al. The Bombora wave energy converter: A novel multi-purpose device for electricity, coastal protection and surf breaks. in Australasian Coasts & Ports Conference 2015: 22nd Australasian Coastal and Ocean Engineering Conference and the 15th Australasian Port and Harbour Conference. 2015. Engineers Australia and IPENZ.
[8] T. Luhmann, S. Robson, S. Kyle, I. Harley, et al, Close range photogrammetry, Wiley, 2007.
[9] B. Hallert, Photogrammetry, basic principles and general survey, 1960.
[10] T. Luhmann, Close range photogrammetry for industrial applications, ISPRS J. Photogramm. Remote Sensing 65 (2010) 558–569.
[11] L.R. Giersch, Pathfinder Photogrammetry Research for Ultra Lightweight and Inflatable Space Structures, NASA Langley Research Center, 2001.
[12] R.S. Pappa, T.W. Jones, J.T. Black, A. Walford, S. Robson, M.R. Shortis, et al., Photogrammetry Methodology for Gossamer Spacecraft Structures, in: American Institute of Aeronautics and Astronautics 3rd Gossamer Spacecraft Conference, 2002, Denver, CO.
[13] J.T. Black, R.S. Pappa, photogrammetry and videogrammetry methods for solar sails and other gossamer structures, NASA Langley Research Center, 2003.
[14] K. Graf, O. Müller, Photogrammetric investigation of the flying shape of spinnakers in a twisted flow wind tunnel, in: The 19th Chesapeake Sailing Yacht Symposium, Annapolis, MD, 2009.
[15] I. Penesis, R. Manasseh, J.-R. Nader, S. De Chowdhury, A. Fleming, G. MacFarlane, M.K. Hasan, et al., Performance of ocean wave-energy arrays in Australia, in: 3rd Asian Wave and Tidal Energy Conference (AWTEC 2016), 2016.
[16] M. Bennet, I. Penesis, A. Fleming, G. Macfarlane, J.-R. Nader, et al., Experimental study into the diffracted wave field downstream of an array of wave energy converters in irregular waves, in: European Wave and Tidal Energy Conference, Cork, Ireland, 2017.
[17] A. Fleming, R. Manasseh, Preliminary experimental observation of surface currents produced by simulating WEC radiation and diffraction wave fields, in: European Wave and Tidal Energy Conference, Cork, Ireland, 2017.
[18] S. Bourdier, K. Dampney, H. Fernandez, G. Lopez, J.-B. Rochon, et al., Report on non-intrusive wave field measurement, in D4.05.2014, MaRINET.
[19] T. Schenk, Introduction to Photogrammetry, The Ohio State University Department of Civil and Environmental Engineering and Geodetic Science, 2005.
[20] PhotoModeler, 2016. Available from: <http://www.photomodeler.com>.
[21] J. Orphin, J.-R. Nader, I. Penesis, D. Howe, et al., Experimental uncertainty analysis of an owc wave energy converter, in: European Wave and Tidal Energy Conference, Cork, Ireland, 2017.
[22] ITTC, Guide to the Expression of Uncertainty in Experimental Hydrodynamics, in: 7.5-02-01-01 2014, International Towing Tank Conference, 2014.
[23] S. Ryan, Bombora Wave Power, 2017, 15/04/17. Available from: <www.bomborawavepower.com.au>.
[24] E. Rupnika, J. Jansab, Off-the-shelf Videogrammetry – A Succes Story, 2014.

Please cite this article in press as: J. Orphin et al., Physical scale model testing of a flexible membrane wave energy converter: Videogrammetric analysis of membrane operation, International Journal of Marine Energy (2017), https://doi.org/10.1016/j.ijome.2017.09.004